Time-Resolved Pulse Propagation in Glass in Single-Shot

Yen-Yu Chang, James Welch, Rafal Zgadzaj, Aaron Bernstein, and Michael C. Downer*
Department of Physics, The University of Texas at Austin, Austin, Texas 78712-1081, USA

Zhengyan Li
University of Ottawa and National Research
(Dated: December 14, 2024)

We report time-resolved pulse self-steepening and temporal splitting in flint glass (SF11) in single-shot using broadband frequency-domain streak camera (B-FDSC). The broadband (60 nm) probe beam generated through a compact coverslip array provides ~ 40 fs temporal resolution. The experimental results support the theoretical model of pulse self-steepening and indicate that multiphoton ionization (MPI) initiates the pulse splitting process in glass. We perform a three-dimensional simulation to verify the experimental results.

I. INTRODUCTION

Nonlinear propagation of ultrashort pulses in transparent materials can induce significant effects on the temporal, spectral, and spatial profile of the pulses. Theory [1] and simulation [2] have shown that when the pulse power is above the critical power for self-focusing (P_{cr}), the pulse will undergo dramatic collapse.

Chernev et al.[3] performed a simulation based on the Nonlinear Schrodinger equation (NLSE), and discovered that when a pulse propagated in normal dispersive material, it temporally split into two symmetric pulses. In that paper, they suggested that the splitting was caused by strong diffraction of the peak of the pulse in the presence of group velocity dispersion (GVD).

Experiments have also provided evidence of pulse temporal splitting in glass. For instance, Diddams et al.[4] measured the temporal profile of pulses propagating through 2.5 cm fused silica and discovered, using SHG-FROG, that temporal splitting occurred when the pulse power $P > P_{cr}$. Multiple reports have suggested that MPI and plasma defocusing is the main cause of pulse temporal splitting in solids. For example, Ranka et al. [5] revealed a close connection between supercontinuum generation (SCG) and pulse temporal splitting in a BK-7 glass window, which indicates that plasma generation may play a key role in pulse splitting. Moreover, Tzortzakis et al. [6] suggested that the mechanism behind the robust filament is the balance between self-focusing and MPI.

In order to fully reveal pulse propagation in transparent materials in single shot, our group has developed a series of spectral interferometry techniques. In frequency-domain holography (FDH)[7], we sent frequency-doubled probe and reference pulses propagate co-linearly with the pump pulse and obtained a snapshot of the pump-induced phase structure in a dispersive material. Using a frequency-domain streak camera (FDSC) [8], we extended FDH by introducing an oblique angle between the beam paths of the pump and the probe beam. Since the group velocity of the pump and the probe are different, the oblique angle converts a 2D phase streak to a time-resolved pump propagation in single-shot. Li et al.[8] have used FDSC to reveal a time-resolved process of pulse self-focusing in glass.

Using frequency-domain tomography (FDT), we apply multiple probe beams simultaneously to overlap with the pump with various angles and obtain a 2D movie of the pump pulse in a single shot. Li et al. [9] have used FDT to reveal that pulse collapsing in 3 mm fused silica was induced by plasma generation. Nevertheless, all the previous methods were not sufficient to resolve pulse temporal splitting because that the temporal resolution was limited by the bandwidth of the probe beam. The temporal resolution of spectral interferometry techniques can be written as $\Delta t_{res} \sim (\Delta\omega)^{-1}[1 + 2\beta_2^2(\Delta\omega)^4]^{1/2}$ [10][11], where $\Delta\omega$ is the frequency bandwidth of the probe, $\beta_2 = 1/2(\partial^2\phi/\partial\omega^2)_{\omega_0}$ is the GVD of the probe. Therefore, in order to obtain the time-resolved process of pulse temporal splitting in single shot by using FDSC, one needs to broaden the bandwidth of the probe beam (to increase $\Delta\omega$).

In this letter, we report, for the first time, time-resolved pulse propagation in 3 mm thick flint glass (SF11) in single shot using a broadband frequency-domain streak camera (B-FDSC). Unlike the conventional FDSC and FDT where the bandwidth of the probe beam was ~ 20 nm, we broadened the bandwidth to ~ 60 nm using supercontinuum generation through a coverslip array. The temporal resolution of B-FDSC was ~ 40 fs. Our measurements revealed the time-resolved process of pulse self-steepening and temporal splitting in single-shot. We performed a simulation that accounts for self-focusing, MPI, GVD, self-steepening, and space-time focusing effects to verify the experimental results.

II. EXPERIMENTAL PROCEDURE

The schematic of the experimental setup is shown in Fig.1. To generate the broadband probe beam, we fo-

* downer@physics.utexas.edu

cused a 800 nm pulse (1 mJ, 40 fs) onto six 100 μm thick glass coverslips with $f/400$ [12]. Each coverslip was rotated to the Brewster angle to yield the maximum transmission. The first coverslip was located close to the focal point of the beam, but one has to finely adjust the positions of the following coverslips to optimize the spectrum of the beam. When propagating through the coverslips, the beam experienced self-focusing and diffraction. Therefore, one had to carefully adjust the distance between the coverslips to maintain the supercontinuum generation throughout the propagation.

Moreover, since spectral interferogram requires a smooth spectrum, one has to adjust the distances between the coverslips to prevent strong spectral modulation of the beam. We monitored the spectrum of the beam as we gradually added the coverslips until the spectrum stopped broadening. In our case, the distances between the coverslips ranged from 1 cm to 3 cm. The bandwidth of the beam extended from 550 nm to 950 nm, while maintaining a smooth and symmetric beam profile (see Fig.1(b)). We then sent the spectral-broadened probe beam through a shortpass filter (cutoff at 670 nm) to select the blue-shifted bandwidth we needed for the experiment. The bandwidth of the beam (FWHM $\sim$ 60 nm) should provide temporal resolution $\Delta t_{res} \sim 40$ fs[10].

After the shortpass filter, we sent the beam through a piece of 3 cm thick BK-7 to chirp the beam to $\sim$ 500 fs and used a Michelson interferometer to generate the separate reference and probe pulses for FDSC measurement[8].

Ideally, the temporal distance (δt) between the reference and the probe pulses needs to be as far as possible to avoid cross-talk[9]. However, δt is limited by the spectral resolution of the spectrometer. The restriction of δt can be derived from fourier transform as $\delta t \leq \lambda_0^2/(c \cdot d\lambda)$, where λ_0 is the central wavelength and $d\lambda$ is the separation of the spectral fringes on the interferogram. The spectral resolution of the spectrometer is $\sim$ 0.11 nm. Consider $d\lambda = 0.55$ nm and $\lambda_0 = 650$ nm, we get $\delta t \leq 2.6$ ps. In the experiment, we used $\delta t = 1.2$ ps.

The pump beam (800 nm, $\tau_L \approx 50$ fs) was synchronized with the probe beam and focused on a 3-mm-thick glass sample ($w_0 \approx 25.5$ μm). In order to acquire large phase shift induced by the pump beam, we used SF11 as the sample material, which has high nonlinear refractive index ($n_2 = 9.5\times10^{-16}$ cm^2/W) and low $P_{cr} = \lambda_0^2/(2\pi n_0 n_2) \approx 0.6$ MW ($n_0 \approx 1.76$). The oblique angle between the beam path of the pump and the probe was 11.95° in the lab frame, and the corresponding probing angle was 73.6° in the probe's co-moving frame, which means that the retrieved phase streak should provide the evolution of the temporal profile of the pump pulse [8].

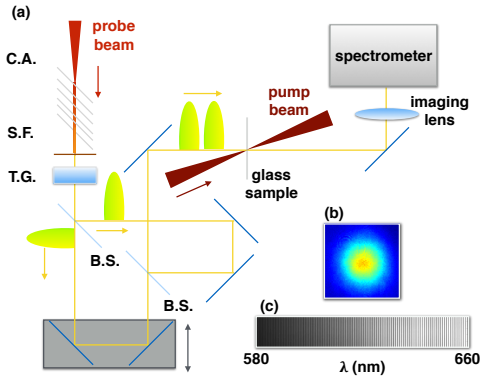

FIG. 1. (a) The layout of the experimental setup. C.A. stands for coverslip array, S.F. stands for shortpass filter, T.G. stands for thick glass, and B.S. stands for beamsplitter. (b) The profile of the probe beam. (c) The null spectral interferogram of the probe and reference pulses.

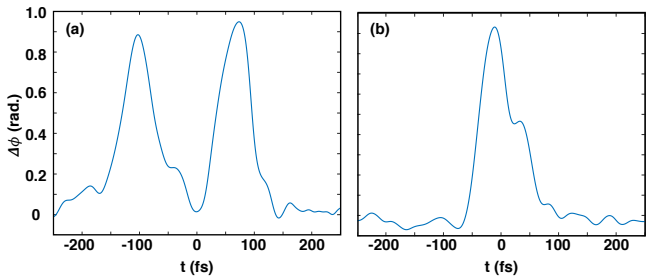

FIG. 2. The test of the temporal resolution of B-FDSC. The phase difference $\Delta\phi$ was induced by two pump pulses co-linearly propagated through 1 mm thick SF11. (a) Two pump pulses are 176 fs away. (b) Two pump pulses are 43 fs away.

III. EXPERIMENTAL RESULTS

Before performing the experiment, we tested the temporal resolution of B-FDSC by sending two pump pulses propagating co-linearly with various temporal separations to a 1 mm thick SF11 glass. The results (see Fig. 2) suggest that the limit of the temporal resolution is around 40 fs.

The experimental results are shown in Fig.3. The top row (Fig.3(a)(c)) is the raw hologram data. The second row (Fig.3(d)(f)) is the phase streak extracted from the hologram. The phase streak in Fig.3 evolves from top to bottom. Since the probing angle in the probe's co-moving frame is close to 90◦, the horizontal lineout of the phase streak represents the temporal profile of the object (the pump pulse). The vertical axis z represents the propagation distance of the object. The left-hand side is the front of the object and the right-hand side is the back. The trace of the phase streak indicates the group velocity of the object. Shallow angle toward the left means that the object propagates quickly, and steep

angle means that the object propagates slowly. The third row (Fig.3(g)(i)) is the spectrum of the pump pulse after exiting the glass sample.

Each column of Fig.3 represents a different pump pulse energy, ranging from 0.8 μJ to 2.4 μJ, and the peak intensity (I_0) of the pulse ranging from 0.78 to 2.34 TW/cm^2. In the first column on the left where $I_0 \sim 0.78$ TW/cm^2, the phase streak shows that the intensity of the pump pulse increased gradually due to self-focusing from the beginning of the entrance until $z \sim 1.3$ mm, after which the leading edge of the pulse started to withdraw and the pulse length became shorter. This phenomenon can be explained by the theory of self-steepening[13][14]. Pulse self-steepening occurs because the velocity of the peak intensity of the pulse is slower than that of the trailing edge of the pulse due to the nonlinear refractive index $\Delta n = n_2 I$. Therefore, as the pulse propagates, the peak and the leading part of the pulse start to withdraw and the trailing part of the pulse gradually catches up and hence shortens the pulse length. Note that on Fig.3(d), the trace of the leading edge and the peak become steeper at $z \sim 1.5$ mm, which means that the velocities of the leading part and the peak of the pulse become slower. This verifies the theory of pulse self-steepening.

On Fig.3(e) where $I_0 \sim 1.56$ TW/cm^2, the pulse self-focused deeper into the sample until $z \sim 1.7$ mm. The turning angle shown on the phase streak indicates that the group velocity of the pump beam suddenly increased, which indicates that the central wavelength of the pulse was redshifted. The estimated central wavelength based on the trace of the phase streak is $\sim$ 820 nm, which is consistent with the exit spectrum of the pump beam, where the spectrum was broadened from 700 to 900 nm and peaked at 820 nm.

Lastly, on Fig.3(f) where $I_0 \sim 2.34$ TW/cm^2, the pulse self-focused quickly until $z \sim 1.2$ mm where the peak intensity suddenly dropped. The decreasing of the peak intensity can be caused by multiphoton absorption (MPA) and plasma defocusing. After the intensity dropped, the pulse temporally split into two pulses which separated further due to different group velocities as indicated in the phase streak. Based on the trace of the phase streak, the center wavelength of the front pulse was 820 nm, and that of the back pulse was 770 nm.

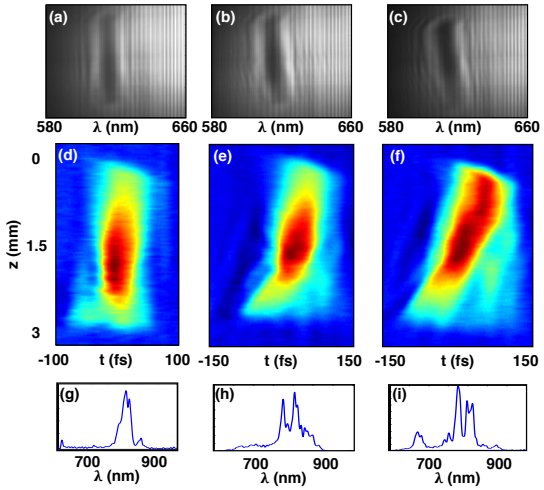

FIG. 3. The experimental results. (a) to (c) The raw hologram data with different pump energies. (d) to (f) The phase streaks extracted from the hologram data. Since the projection angle is close to 90° in the probe frame, the horizontal lineout represents the temporal profile of the pump pump pulse. (g) to (i) The spectra of the pump pulse after propagating through the SF11 glass sample. The pump energies are 0.88, 1.76, and 2.4 μJ from the left column to the right column.

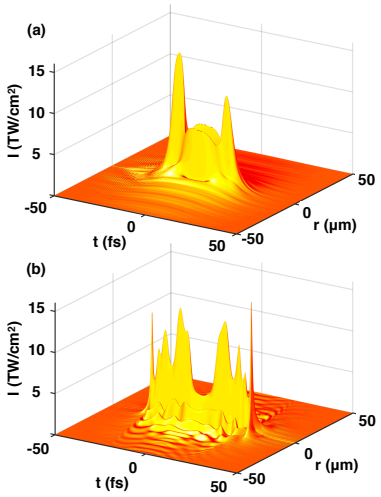

FIG. 4. The surface plot of the intensity of the pulse in the simulation. (a) The pulse intensity when $z = 0.94$ mm. (b) The pulse intensity when $z = 1.6$ mm.

IV. SIMULATION

To explain the experimental results, we performed a 3D cylindrical symmetric simulation to demonstrate pulse propagation in SF11. The simulation included an extended NLSE, coupled with the density of electrons produced by MPI without avalanche onization. We assumed that the pulse was cylindrically symmetric and linearly polarized with central wavelength $\lambda_0 = 800$ nm. The electric field of the pulse was given as

$$\mathbf{E}(r,t,z) = \sqrt{I_0} exp(-(\frac{r}{w_0})^2 - (\frac{t}{\tau_0})^2),$$

where $I_0 = 1.8$ TW/cm^2, $w_0 = 30$ μm , and $\tau_0 = 50$ fs.The parameters in the simulation were chosen to match the pump beam that generated pulse splitting in the experiment when it focused on the target.

The electric field of the beam evolved according to

$$\frac{\partial \mathbf{E}}{\partial z} = \frac{i}{2k_0 n_0} T^{-1}(\frac{\partial^2}{\partial r^2} + \frac{\partial}{r\partial r})\mathbf{E} - \frac{ik''}{2}\frac{\partial^2 \mathbf{E}}{\partial \tau^2} + ik_0 n_2 T(\|E^2\|\mathbf{E}) - \frac{ik_0}{2n_0\rho_c} T^{-1}(\rho \mathbf{E}) - \frac{1}{2}\beta^{(K)}\|E\|^{(2K-2)}\mathbf{E}, \quad (1)$$

where τ is the retarded time variable $t - z/v_g$ with group velocity v_g. The first term on the right hand side describes the diffraction of the beam in the transverse plane, and the operator $T = 1 + (i/\omega_0)\partial/\partial\tau$ accounts for space-time focusing and self-steepening of the pulse[2]. Here n_0 is 1.76, and $k_0 = 2\pi c/\lambda_0$ ($\lambda_0 = 0.8$ μm). The second term describes pulse dispersion with $k'' = 187.5\ fs^2/cm$ as the GVD coefficient. The third term accounts for Kerr self-focusing, and $n_2 = 9.5\times10^{-20}$ m^2/W is the nonlinear refractive index, obtained by performing a z-scan separately. The fourth term represents plasma defocusing [**?**], where $\rho_c = 1.8 \times 10^{21}$ cm^{-3} is the critical density, and ρ is the plasma density. The last term describes MPA where $\beta^{(K)} = K\hbar\omega_0\sigma_K\rho_{at}$[6]. Since the gap potential of the sample material is $U_i = 3.3$ eV [15], $K = 3$ in this case. Here $\rho_{at} = 2.1\times10^{22}$ atoms/cm^3 is the background atom density of the glass sample, and σ_K is chosen to fit the data, which will be explained later.

The evolution equation for the electron density is

$$\frac{\partial \rho}{\partial \tau} = \sigma_K \|E\|^{2K}(\rho_{at} - \rho) - \frac{\rho}{\tau_r}, \quad (2)$$

where the first term on the right hand side describes the photoionization contribution to the electron generation. The second term accounts for electron recombination with a characteristic time $\tau_r = 25$ fs, which is obtained by performing the methods demonstrated by Sun et al. [16].

In order to determine σ_K, we estimated the multiphoton absorption length (L_{MPA}) of SF11 [17] defined as the length over which the intensity of the pulse I is attenuated by a factor of $[(K+1)/2]^{(K-1)}$. L_{MPA} can be written as

$$L_{MPA} = \frac{1}{2K\hbar\omega_0\sigma_K\rho_{at}I^{K-1}}$$

Based on the experimental results, we estimate that L_{MPA} ranges from 50 to 200 μm, which means σ_K ranges between 1.6 and 6.4×10^7 s^{-1}[TW/cm^2]^3. We scan the value of σ_K in the simulation and discover that $\sigma_K = 3.2 \times 10^7$ s^{-1}[TW/cm^2]^3 can best fit the experimental results. The corresponding L_{MPA} is 100 μ m.

The simulation results is shown in Fig.4. The beam self-focuses when it enters the glass and starts to temporally collapse into two pulses at $z = 0.94$ mm due to MPA (see Fig.4(a)), which is close to where the pulse collapsed in the experiment. The pulse at the front appears to have stronger intensity than the one in the back, which is consistent with the observation in the experiment. Afterwards, the split pulses start to modulate can generate multiple filaments as shown in Fig. 4(b).

V. CONCLUSION

In sum, we have demonstrated time-resolved process of pulse self-steepening and pulse temporal splitting in single shot using a B-FDSC. The experimental results verified the theory of pulse self-steepening and suggested that MPI and plasma defocusing initiated the pulse temporal splitting. We performed a three-dimensional simulation to support the experimental results.

[1] J. H. Marburger, Progress in Quantum Electronics , 35 (1975).
[2] A. Gaeta, Physical Review Letters **84**, 3582 (2000).
[3] P.Chernev and V. Petrov, Optics Letters **17**, 172 (1992).
[4] S. Diddams, H. Eaton, A. Zozulya, and T. Clement, Optics Letters **23**, 379 (1998).
[5] J. Ranka, R. Schirmer, and A. Gaeta, Physical Review Letters **77**, 3783 (1996).
[6] S. Tzortzakis, L. Sudrie, M. Franco, B. Prade, and A. Mysyrowicz, Physics Review Letters **87**, 19 (2001).
[7] N. Matlis, S. Reed, S. Bulanov, V. Chvykov, G. Kalintchenko, T. Matsuoka, P. Rousseau, V. Yanovsky, A. Maksimchuk, S. Kalmykov, G. Shvets, and M. Downer, Nature Physics **2**, 749 (2006).
[8] Z. Li, R. Zgadzaj, X. Wang, S. Reed, P. Dong, and M. Downer, Optics Letters **35**, 4087 (2010).
[9] Z. Li, R. Zgadzaj, X. Wang, Y. Chang, and M. Downer, Nature Communications **5**, 3085 (2014).
[10] K. Kim, I. Alexeev, and H. Milchberg, Applied Physics Letters **81**, 4124 (2002).
[11] E. Tokunaga, A. Terasaki, and T. Kobayashi, Journal of the Optical Society of America B **13**, 496 (1996).
[12] C. Lu, Y. Tsou, H. Y. Chen, B. Chen, Y. Cheng, S. D. Yang, M. C. Chen, C. Hsu, and A. H. Kung, Optica **1**, 10 (2014).
[13] D. Anderson and M. Lisak, Physical Review A **27**, 1393 (1983).
[14] J. Rothenberg, Optics Letters **17**, 1340 (1992).
[15] C. Schaffer, A. Brodeur, and E. Mazur, Measurement Science and Technology **12**, 1784 (2001).
[16] Q. Sun, H. Jiang, Y. Liu, Z. Wu, H. Yang, and Q. Gong, Optics Letters **30**, 320 (2005).
[17] A. Couairon and A. Mysyrowicz, Physics Reports **30**, 47 (2007).